

Supplementary Material for ‘Topological Magnons in the Kitaev Honeycomb Model at High Fields’

P. A. McClarty,¹ X.-Y. Dong,¹ M. Gohlke,¹ J. G. Rau,¹ F. Pollmann,² R. Moessner,¹ and K. Penc^{1,3}

¹Max Planck Institute for the Physics of Complex Systems, Nöthnitzer Str. 38, 01187 Dresden

²Physics Department, Technical University Munich, James-Frank-Str. 1, 85748 Garching

³Institute for Solid State Physics and Optics, Wigner RCP, P.O.B. 49, H-1525 Budapest, Hungary

I. SYMMETRY-ALLOWED EXCHANGE HAMILTONIAN

Here we will derive the symmetry allowed terms for the edge-shared octahedral compounds (see also Ref. 1 and 2). The Ir⁴⁺ and Ru³⁺ in the center of oxygen octahedra forms a honeycomb lattice. Taking into account the octahedral environment, the symmetry group of a single bond consists of the inversion, the two-fold rotation around the bond, and their composition, a mirror plane which is perpendicular to the bond. The point group at the center of the hexagon is D_{3d} , generated by the S_6 roto-reflection (we note that S_6^3 is the inversion) and the mirror plane. The point group at the Ir site is D_3 , with a C_3 threefold rotation and a C_2' rotation as generators.

First, let us consider the x bond in the geometry presented in Fig. 1. The inversion at the center of the bond exchanges the two sites without affecting the spin components, $\mathbf{S}_1^\alpha \leftrightarrow \mathbf{S}_2^\alpha$. The C_2 rotation does not exchange the sites; it acts only on the spin components as $\mathbf{S}^x \rightarrow -\mathbf{S}^x$ [the \mathbf{S}^α component of the spin is perpendicular to the $\alpha = x, y, z$ bond and, with the constraint that the components form an orthogonal basis, there are eight possible choices of axis convention out of which we have chosen one (Fig. 1)], $\mathbf{S}^y \rightarrow -\mathbf{S}^z$, and $\mathbf{S}^z \rightarrow -\mathbf{S}^y$. We can construct the following 4 invariants:

$$\mathbf{S}_1^x \mathbf{S}_2^x, \tag{1}$$

$$\mathbf{S}_1^y \mathbf{S}_2^y + \mathbf{S}_1^z \mathbf{S}_2^z \tag{2}$$

$$\mathbf{S}_1^z \mathbf{S}_2^y + \mathbf{S}_1^y \mathbf{S}_2^z, \tag{3}$$

$$\mathbf{S}_1^x \mathbf{S}_2^y + \mathbf{S}_1^x \mathbf{S}_2^z + \mathbf{S}_1^y \mathbf{S}_2^x + \mathbf{S}_1^z \mathbf{S}_2^x. \tag{4}$$

Adding them up with a suitable coefficients we arrive to

$$\begin{aligned} \mathcal{H}_x = & 2K \mathbf{S}_1^x \mathbf{S}_2^x + J \mathbf{S}_1 \cdot \mathbf{S}_2 + \Gamma (\mathbf{S}_1^z \mathbf{S}_2^y + \mathbf{S}_1^y \mathbf{S}_2^z) \\ & + \Gamma' (\mathbf{S}_1^x \mathbf{S}_2^y + \mathbf{S}_1^x \mathbf{S}_2^z + \mathbf{S}_1^y \mathbf{S}_2^x + \mathbf{S}_1^z \mathbf{S}_2^x) \end{aligned} \tag{5}$$

The inversion symmetry about the bond centers prevents DM interactions.

Next, we use the C_3 rotation about site 1 to get the Hamiltonian for the y bond, as it cyclically exchanges the three spin components, $\mathbf{S}^x \rightarrow \mathbf{S}^y \rightarrow \mathbf{S}^z \rightarrow \mathbf{S}^x$, furthermore site 1 remains, and site 2 becomes site 3:

$$\begin{aligned} \mathcal{H}_y = & 2K \mathbf{S}_1^y \mathbf{S}_3^y + J \mathbf{S}_1 \cdot \mathbf{S}_3 + \Gamma (\mathbf{S}_1^x \mathbf{S}_3^z + \mathbf{S}_1^z \mathbf{S}_3^x) \\ & + \Gamma' (\mathbf{S}_1^y \mathbf{S}_3^z + \mathbf{S}_1^y \mathbf{S}_3^x + \mathbf{S}_1^z \mathbf{S}_3^y + \mathbf{S}_1^x \mathbf{S}_3^y), \end{aligned} \tag{6}$$

and a similar form for the \mathcal{H}_z . This is the Hamiltonian first established in Refs. 1–4.

II. LINEAR SPIN WAVE THEORY

The honeycomb lattice is triangular $\mathbf{R}_{mn} = (m - (n/2), \sqrt{3}n/2)$ with a two site basis. We take the bonds to be

$$\begin{aligned} \delta_x &= (0, 1), \\ \delta_y &= \left(-\frac{\sqrt{3}}{2}, -\frac{1}{2} \right), \\ \delta_z &= \left(\frac{\sqrt{3}}{2}, -\frac{1}{2} \right), \end{aligned}$$

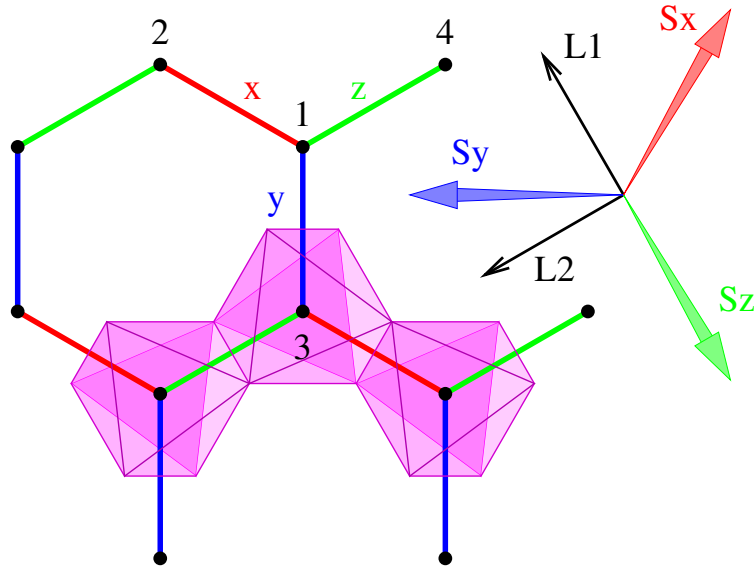


FIG. 1. Schematic of the lattice structure: the magnetic sites (black circles) in octahedral environment (magenta) form a honeycomb lattice. The x (red bonds), y (blue), and z (green) Kitaev interactions are indicated. The spin components S^x , S^y , and S^z form an orthogonal bases, shown on the right. $L^{(1)}$ and $L^{(2)}$ are the two components of rotated spins used to derive the spin wave Hamiltonian, when the $L^{(3)}$ is perpendicular to the honeycomb plane and parallel to the external field direction $[111]$. The numbers 1,2,3, and 4 denote lattice sites used in the text.

As outlined in the main text, we can define the following vector of the bosonic operators

$$\Upsilon_{\mathbf{k}} = (a_{\mathbf{k}}, b_{\mathbf{k}}, a_{-\mathbf{k}}^{\dagger}, b_{-\mathbf{k}}^{\dagger}). \quad (7)$$

Then the linear spin wave Hamiltonian can also be cast into the form

$$\mathcal{H}_{\text{LSW}} = \frac{1}{2} \sum_{\mathbf{k} \in \text{BZ}} \Upsilon_{\mathbf{k}}^{\dagger} \cdot \mathbf{H}_{\text{LSW}}(\mathbf{k}) \cdot \Upsilon_{\mathbf{k}} \quad (8)$$

For the Kitaev-Heisenberg model we find [5]

$$\mathbf{H}_{\text{KH-LSW}}(\mathbf{k}) = \begin{pmatrix} \mathbf{A}(\mathbf{k}) & \mathbf{B}(\mathbf{k}) \\ \mathbf{B}^{\dagger}(\mathbf{k}) & \mathbf{A}^T(-\mathbf{k}) \end{pmatrix} \quad (9)$$

where

$$\mathbf{A}(\mathbf{k}) = \begin{pmatrix} -3JS - 2KS + h & (J + \frac{2K}{3})S (e^{ik\cdot\delta_x} + e^{ik\cdot\delta_y} + e^{ik\cdot\delta_z}) \\ (J + \frac{2K}{3})S (e^{-ik\cdot\delta_x} + e^{-ik\cdot\delta_y} + e^{-ik\cdot\delta_z}) & -3JS - 2KS + h \end{pmatrix} \quad (10)$$

$$\mathbf{B}(\mathbf{k}) = \begin{pmatrix} 0 & \frac{2KS}{3} (e^{ik\cdot\delta_x + \frac{2\pi i}{3}} + e^{ik\cdot\delta_y - \frac{2\pi i}{3}} + e^{ik\cdot\delta_z}) \\ \frac{2KS}{3} (e^{-ik\cdot\delta_x + \frac{2\pi i}{3}} + e^{-ik\cdot\delta_y - \frac{2\pi i}{3}} + e^{-ik\cdot\delta_z}) & 0 \end{pmatrix} \quad (11)$$

In the main text, we parametrized the couplings using ϑ such that $J = \cos \vartheta$ and $K = \sin \vartheta$.

It is convenient to introduce

$$\gamma_{0,\mathbf{k}} = \frac{1}{3} (e^{-ik\cdot\delta_x} + e^{-ik\cdot\delta_y} + e^{-ik\cdot\delta_z}), \quad (12)$$

$$\gamma_{1,\mathbf{k}} = \frac{1}{3} (e^{-ik\cdot\delta_x - (2\pi i/3)} + e^{-ik\cdot\delta_y + (2\pi i/3)} + e^{-ik\cdot\delta_z}), \quad (13)$$

$$\gamma_{2,\mathbf{k}} = \frac{1}{3} (e^{-ik\cdot\delta_x + (2\pi i/3)} + e^{-ik\cdot\delta_y - (2\pi i/3)} + e^{-ik\cdot\delta_z}), \quad (14)$$

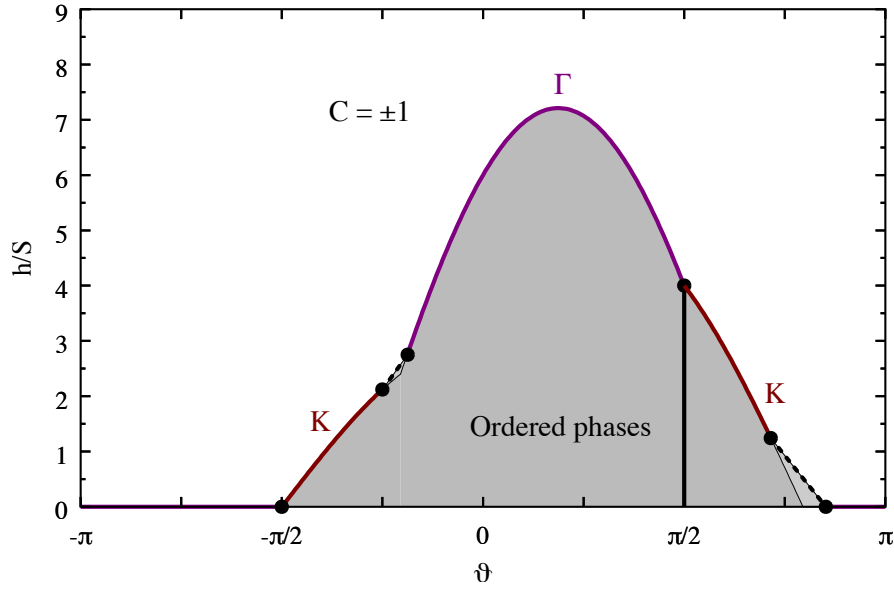


FIG. 2. The phase diagram of the Kitaev-Heisenberg model as a function of ϑ and h/S . The solid line phase boundary is the linear spin wave instability upon lowering h . The instabilities into long-range ordered magnetic phases occur at the indicated locations in the Brillouin zone. This figure differs from the one in the main text in showing dashed lines which are first-order transition lines not captured by linear spin wave theory – they appear instead in the classical model at finite temperature and were taken from Refs. 5 and 6.

satisfying the relations $\gamma_{0,k}^* = \gamma_{0,-k}$, $\gamma_{1,k}^* = \gamma_{2,-k}$, and $\gamma_{2,k}^* = \gamma_{1,-k}$ so that

$$\mathbf{A}(\mathbf{k}) = h \begin{pmatrix} 1 & 0 \\ 0 & 1 \end{pmatrix} + (3J + 2K)S \begin{pmatrix} -1 & \gamma_{0,k}^* \\ \gamma_{0,k} & -1 \end{pmatrix}, \quad (15)$$

$$\mathbf{B}(\mathbf{k}) = 2KS \begin{pmatrix} 0 & \gamma_{1,k}^* \\ \gamma_{2,k} & 0 \end{pmatrix}. \quad (16)$$

A. Mapping $\vartheta \rightarrow \vartheta + \pi$

Under the mapping $\vartheta \rightarrow \vartheta + \pi$, the couplings flip sign. There is a simple relationship between the spectra of the linear spin wave Hamiltonian under this mapping when combined with a field redefinition $h \rightarrow h - 6JS - 4KS$, that preserves the diagonal matrix elements, and $\mathbf{k} \rightarrow -\mathbf{k}$. This whole transformation can be undone by a unitary transformation of the form

$$\begin{pmatrix} 0 & 1 & 0 & 0 \\ -1 & 0 & 0 & 0 \\ 0 & 0 & 0 & 1 \\ 0 & 0 & -1 & 0 \end{pmatrix}.$$

It follows that, under the mapping, as measured from the threshold field the spectrum is left unchanged.

B. The Role of the Γ and Γ' Terms

The Γ and Γ' terms are symmetric exchange couplings that are allowed by the symmetries of the honeycomb lattice as discussed above.

For fully polarized moments in the [111] direction, the Γ and Γ' couplings merely effect the following mapping on the J, K, h model:

$$K \rightarrow K + \Gamma - \Gamma', \quad (17a)$$

$$J \rightarrow J - \Gamma, \quad (17b)$$

$$h \rightarrow h - 3\Gamma S - 6\Gamma' S. \quad (17c)$$

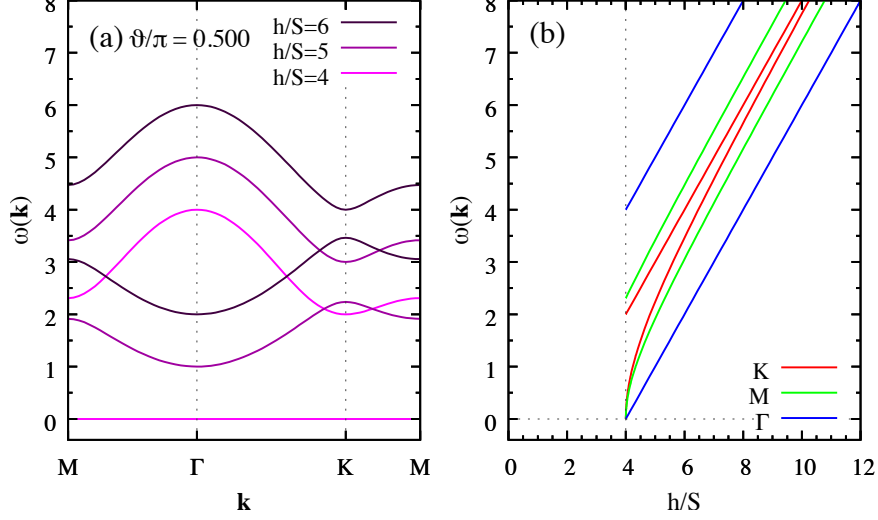


FIG. 3. (a) Magnon dispersion relations along high symmetry lines, as marked in the upper panel, for three different fields $h/S = 4, 5, 6$ at the isotropic AFM point $\vartheta = 0$. Panel (b) shows the spin wave energies as a function of field at three high symmetry points, illustrating the linear dependence of the lowermost mode at the Γ , K and M points.

In other words, all the results we obtained for the Kitaev-Heisenberg model can be extended to the $JKT\Gamma'$ model using the replacement rules above.

C. The canonical transformation

In this section, we examine the linear spin wave theory at high fields and systematically integrate out the number non-conserving terms in powers of $1/h$ to obtain an effective hopping Hamiltonian for the magnons.

To proceed, we look for a canonical transformation

$$\begin{aligned} \mathcal{H}_{\text{eff}} &= e^{\mathcal{W}} \mathcal{H} e^{-\mathcal{W}} \\ &= \mathcal{H} + [\mathcal{W}, \mathcal{H}] + \frac{1}{2} [\mathcal{W}, [\mathcal{W}, \mathcal{H}]] + \dots \end{aligned} \quad (18)$$

where the operator \mathcal{W} is chosen such that the transformation eliminates the magnon number non-conserving anomalous terms to $O(1/h)$ instead capturing their effect to this order in terms of a pure hopping Hamiltonian. This is achieved by choosing

$$\mathcal{W} = \frac{KS}{h} \sum_{k \in \text{BZ}} (\gamma_{1,k}^* a_k^\dagger b_{-k}^\dagger - \gamma_{1,k} a_k b_{-k}), \quad (19)$$

or, in the matrix notation we used above (Eq. 8) for the linear spin wave Hamiltonian,

$$\mathcal{W}(\mathbf{k}) = \frac{1}{2h} \begin{pmatrix} 0 & \mathbf{B}(\mathbf{k}) \\ -\mathbf{B}^\dagger(\mathbf{k}) & 0 \end{pmatrix}. \quad (20)$$

The effective Hamiltonian is then characterized by the

$$\mathbf{A}_{\text{eff}}(\mathbf{k}) = \mathbf{A}(\mathbf{k}) - \frac{2K^2 S^2}{h} \begin{pmatrix} \gamma_{1,k}^* \gamma_{1,k} & 0 \\ 0 & \gamma_{2,k}^* \gamma_{2,k} \end{pmatrix}, \quad (21)$$

$$\mathbf{B}_{\text{eff}}(\mathbf{k}) = -\frac{K(3J+2K)S^2}{h} \begin{pmatrix} \gamma_{0,k} \gamma_{1,k}^* + \gamma_{0,k}^* \gamma_{2,k} & -2\gamma_{1,k}^* \\ -2\gamma_{2,k} & \gamma_{0,k} \gamma_{1,k}^* + \gamma_{0,k}^* \gamma_{2,k} \end{pmatrix}, \quad (22)$$

matrices. The canonical transformation generates an onsite correction and a second neighbor Dzyaloshinskii-Moriya term $\propto K^2 S^2/h$ in the $\mathbf{A}_{\text{eff}}(\mathbf{k})$. The anomalous term $\mathbf{B}_{\text{eff}}(\mathbf{k})$ is $1/h$ and can be safely neglected in high fields, so the problem reduces to

the diagonalization of the $\mathbf{A}_{\text{eff}}(\mathbf{k})$ 2×2 matrix. The energies of the magnon excitations of the 4×4 and the effective 2×2 problem are identical including the $1/h$ corrections.

We note in passing that the matrix corresponding to the commutator of operators $[\mathcal{W}, \mathcal{H}]$ is

$$\mathbf{W} \cdot \boldsymbol{\eta} \cdot \mathbf{H} - \mathbf{H} \cdot \boldsymbol{\eta} \cdot \mathbf{W}. \quad (23)$$

D. Chern Number

The $\mathbf{A}_{\text{eff}}(\mathbf{k})$ we need to diagonalize can be expressed as

$$\mathbf{A}_{\text{eff}} = d_0(\mathbf{k})\mathbf{1} + \frac{1}{2}\mathbf{d}(\mathbf{k}) \cdot \boldsymbol{\sigma}, \quad (24)$$

where

$$d_0(\mathbf{k}) = h - (3J + 2K)S - \frac{K^2 S^2}{h} (\gamma_{1,k}^* \gamma_{1,k} + \gamma_{2,k}^* \gamma_{2,k}), \quad (25)$$

and

$$\mathbf{d}(\mathbf{k}) = \begin{pmatrix} (3J + 2K)S(\gamma_{0,k}^* + \gamma_{0,k}) \\ i(3J + 2K)S(\gamma_{0,k}^* - \gamma_{0,k}) \\ -\frac{2K^2 S^2}{h} (\gamma_{1,k}^* \gamma_{1,k} - \gamma_{2,k}^* \gamma_{2,k}) \end{pmatrix}. \quad (26)$$

The $\boldsymbol{\sigma} = (\sigma^x, \sigma^y, \sigma^z)$ is a vector of the Pauli matrices, so the $\mathbf{d}(\mathbf{k})$ acts as a fictitious magnetic field in the Brillouin zone. At each \mathbf{k} we have the eigenvalues

$$\omega_{\pm}(\mathbf{k}) = d_0(\mathbf{k}) \pm \frac{1}{2}d(\mathbf{k}), \quad (27)$$

where $d(\mathbf{k}) = |\mathbf{d}(\mathbf{k})|$. Each of these eigenvalues forms a band in the Brillouin zone, with the spacing between the bands given by $d(\mathbf{k})$. The two bands can only touch when $|d(\mathbf{k})| = 0$, which happens if $K = 0$ or $3J + 2K = 0$.

The Berry curvature for the 2×2 problem is given by

$$F_{\pm}^{xy}(\mathbf{k}) = \pm \frac{i}{2} \frac{\mathbf{d}(\mathbf{k})}{d(\mathbf{k})^3} \cdot \left(\frac{\partial \mathbf{d}(\mathbf{k})}{\partial k_y} \times \frac{\partial \mathbf{d}(\mathbf{k})}{\partial k_x} \right) \quad (28)$$

$$= \pm \frac{i}{2} \hat{\mathbf{d}}(\mathbf{k}) \cdot \left(\frac{\partial \hat{\mathbf{d}}(\mathbf{k})}{\partial k_y} \times \frac{\partial \hat{\mathbf{d}}(\mathbf{k})}{\partial k_x} \right), \quad (29)$$

where $\hat{\mathbf{d}}(\mathbf{k}) = \mathbf{d}(\mathbf{k})/d(\mathbf{k})$ is a unit vector. The Chern number of the band \pm is then

$$C_{\pm} = \frac{1}{2\pi i} \int_{\text{BZ}} dk_x dk_y F_{\pm}^{xy} = \pm N_s, \quad (30)$$

where N_s measures the number of skyrmions (topological defects) in the \mathbf{d} field, as it follows from Eq. (29).

In the case of the Kitaev-Heisenberg model, introducing the notation

$$\begin{aligned} u_c(\mathbf{k}) &= \cos \mathbf{k} \cdot (\boldsymbol{\delta}_z - \boldsymbol{\delta}_y) + \cos \mathbf{k} \cdot (\boldsymbol{\delta}_x - \boldsymbol{\delta}_z) + \cos \mathbf{k} \cdot (\boldsymbol{\delta}_y - \boldsymbol{\delta}_x), \\ u_s(\mathbf{k}) &= \sin \mathbf{k} \cdot (\boldsymbol{\delta}_z - \boldsymbol{\delta}_y) + \sin \mathbf{k} \cdot (\boldsymbol{\delta}_x - \boldsymbol{\delta}_y) + \sin \mathbf{k} \cdot (\boldsymbol{\delta}_z - \boldsymbol{\delta}_y), \end{aligned} \quad (31)$$

the expressions in the Berry curvature, Eq. (28), are

$$\mathbf{d} \cdot \left(\frac{\partial \mathbf{d}}{\partial k_y} \times \frac{\partial \mathbf{d}}{\partial k_x} \right) = -\frac{4(3J+2K)^2 K^2 S^4}{27h} \left[(3 - u_c(\mathbf{k}))^2 - u_s^2(\mathbf{k}) \right], \quad (32)$$

$$d^2 = \frac{4}{9}(3J+2K)^2 S^2 (3 + 2u_c(\mathbf{k})) + \frac{16}{27} \frac{K^4}{h^2} u_s^2(\mathbf{k}). \quad (33)$$

The triple product, Eq. (32), is negative semidefinite in the whole Brillouin zone (it is 0 for $\mathbf{k} = 0$). The Chern number is therefore always finite, apart from the cases when $K = 0$ (the Heisenberg model), and when $3J + 2K = 0$. In large fields, the $F_{\pm}^{xy}(\mathbf{k})$ is strongly peaked at the K points, the corners of the hexagonal Brillouin zone.

E. Thermal Hall conductivity

In this section, we apply the expression for thermal conductivity

$$\tilde{\kappa}^{xy} = \frac{1}{\beta} \sum_{n=\pm} \int_{\text{BZ}} d^2 \mathbf{k} c_2(\rho_n) \frac{F_n^{xy}(\mathbf{k})}{i}, \quad (34)$$

derived by Matsumoto et al. [7], to the case of the Kitaev model. $\beta = 1/T$ is the inverse temperature and

$$\begin{aligned} \rho_n &= \frac{1}{e^{\omega_n \beta} - 1}, \\ c_2(\rho) &= \int_0^\rho dt \ln^2(1 + t^{-1}). \end{aligned} \quad (35)$$

The dimensionful thermal Hall conductivity per layer is $(k_B^2/\hbar)\tilde{\kappa}^{xy}$. Since the upper and lower bands have Berry curvatures with opposite signs, $F_+^{xy}(\mathbf{k}) = -F_-^{xy}(\mathbf{k})$, the expression for the thermal Hall effect simplifies to

$$\tilde{\kappa}^{xy} = \int_{\text{BZ}} d^2 \mathbf{k} \frac{c_2(\rho_+) - c_2(\rho_-)}{\beta} \frac{\mathbf{d}(\mathbf{k})}{d(\mathbf{k})^3} \cdot \left(\frac{\partial \mathbf{d}(\mathbf{k})}{\partial k_y} \times \frac{\partial \mathbf{d}(\mathbf{k})}{\partial k_x} \right). \quad (36)$$

Since in large magnetic field the band dispersions and splittings are much smaller than the gap between the bands and the ground state, $\omega_+ - \omega_- \ll d_0$, we expand Eq. (36) in d/d_0 :

$$\begin{aligned} c_2(\rho_+) - c_2(\rho_-) &= \int_{\rho_-}^{\rho_+} dt \ln^2(1 + t^{-1}), \\ &\approx (\rho_+ - \rho_-) (d_0 \beta)^2, \end{aligned} \quad (37)$$

where the difference of Bose occupation numbers is

$$\rho_+ - \rho_- = -\frac{d\beta}{2 \sinh^2(\frac{d_0 \beta}{2})} + O(d^3), \quad (38)$$

so that

$$\frac{1}{\beta} [c_2(\rho_+) - c_2(\rho_-)] \approx -\frac{(d_0 \beta)^2}{2 \sinh^2(\frac{d_0 \beta}{2})} d. \quad (39)$$

Eventually, we get the following simple expression for the thermal Hall conductivity:

$$\tilde{\kappa}^{xy} = R(d_0 \beta) \tilde{\kappa}_\infty^{xy}, \quad (40)$$

where

$$R(x) = \left(\frac{x}{2 \sinh \frac{x}{2}} \right)^2 \quad (41)$$

and

$$\begin{aligned} \tilde{\kappa}_\infty^{xy} &= \int_{\text{BZ}} d^2 \mathbf{k} \frac{2}{d(\mathbf{k})^2} \mathbf{d}(\mathbf{k}) \cdot \left(\frac{\partial \mathbf{d}(\mathbf{k})}{\partial k_x} \times \frac{\partial \mathbf{d}(\mathbf{k})}{\partial k_y} \right), \\ &= 16\pi \frac{S^2 K^2}{h} \ln \frac{cK^2 S}{h|3J + 2K|} + \dots \end{aligned} \quad (42)$$

in the leading order in $1/h$, where c is a constant of order unity. The temperature dependence stems purely from $R(d_0 \beta)$. At low temperatures, the temperature dependence is thermally activated, while at high temperatures $R \rightarrow 1$ and the conductivity saturates, with $\tilde{\kappa}_\infty^{xy}$ being the high temperature value.

In Fig. 4 in the main text, we show the low temperature thermal Hall conductivity as computed from Eq. 34.

III. NON-LINEAR SPIN-WAVE THEORY

In this section we outline the calculation of the dynamical structure factor in non-linear spin-wave theory. The starting point is the Holstein-Primakoff expansion [8], organized in powers of $1/S$ (factoring out the overall S^2 scaling). Linear spin wave theory appears when truncating to $O(1/S)$. To go to $O(1/S^2)$, one must consider the effects of magnon-magnon interactions, including three- and four-body terms in the Holstein-Primakoff bosons (magnons).

The dynamical structure factor at $O(1/S^2)$ requires the computation of the magnon Green's function as well as several higher order dynamical correlation functions. It is useful to consider three distinct pieces: the transverse-transverse part which involves only the magnon Green's function, $\mathbf{G}(\mathbf{k}, \omega)$, the transverse-longitudinal parts which involve three-magnon correlation functions and the longitudinal-longitudinal parts which involve four-magnon correlation functions [9]. While the transverse-transverse part has $O(1/S)$ contributions, the other two parts appear first at $O(1/S^2)$. We note that the Green's function also appears in the transverse-longitudinal part of the dynamical structure factor, while the longitudinal-longitudinal part involves only the free magnon Green's function at leading order [9].

Typically, the transverse-longitudinal and longitudinal-longitudinal parts are small relative to the leading transverse-transverse contributions. The central ingredient is then (retarded) magnon Green's function [10]

$$\mathbf{G}(\mathbf{k}, \omega) = [(\omega + i0^+)\boldsymbol{\eta} - \mathbf{M}(\mathbf{k}) - \boldsymbol{\Sigma}_{\mathbf{M}}(\mathbf{k}, \omega)]^{-1}, \quad (43)$$

where $\mathbf{M}(\mathbf{k})$ is the linear magnon dispersion matrix (see Eq. (2) of the main text) and $\boldsymbol{\eta} = \text{diag}(+1, -1)$ is due to the bosonic Bogoliubov transformation [10]. The self-energy, $\boldsymbol{\Sigma}_{\mathbf{M}}(\mathbf{k}, \omega)$, appears due to the magnon-magnon interactions and can be evaluated perturbatively in powers of $1/S$, starting from the solution of the linear spin-wave problem encoded in $\mathbf{M}(\mathbf{k})$. This Green's function and the self-energy are both matrices with sublattice indices and have both normal and anomalous contributions [10, 11].

We identify two distinct types of contributions to the self-energy: static (frequency independent) and dynamic (frequency dependent). The static contributions arise from Hartree-Fock-like diagrams involving the four-magnon interactions as well as (in principle) tadpole-like diagrams arising from the three-magnon interaction. The dynamic contributions arise purely from the three-magnon interactions. In addition to renormalizing the one-magnon spectrum they are also responsible for magnon decay [11, 12], possibly endowing the one-magnon states with finite lifetimes.

The Holstein-Primakoff expansion is formally controlled in $1/S$, and is thus a systematic approximation scheme when $S \gg 1$. Alternatively, it can be viewed as an expansion in the magnon density $\rho \equiv \langle a^\dagger a \rangle / (2S)$, and is controlled in the limit, $\rho \ll 1$. For arbitrary S this limit can be reached systematically through the application of a large magnetic field. For small S or for small fields however its validity is more limited. Carried to order $O(1/S^2)$ two key issues are apparent: (a) it is confined by the classical phase boundaries and (b) the two-magnon spectrum does not reflect the renormalization of the one-magnon spectrum due to interactions. While one could alleviate some of these issues by proceeding to higher order in $1/S$, the technical complexity of such calculations is prohibitive both computationally and analytically.

Instead, we adopt a self-consistent approach, allowing the static part the Green's function to renormalize the linear spin-wave dispersion. Specifically, we introduce a renormalization

$$\mathbf{G}(\mathbf{k}, \omega) = [(\omega + i0^+)\boldsymbol{\eta} - \mathbf{M}_{\text{eff}}(\mathbf{k}) - (\boldsymbol{\Sigma}_{\mathbf{M}_{\text{eff}}}(\mathbf{k}, \omega) - \delta\mathbf{M}(\mathbf{k}))]^{-1}, \quad (44)$$

where $\mathbf{M}_{\text{eff}}(\mathbf{k}) \equiv \mathbf{M}(\mathbf{k}) + \delta\mathbf{M}(\mathbf{k})$ and we take (formally) $\delta\mathbf{M}(\mathbf{k}) \sim O(1/S^2)$. Note that the self-energy is evaluated using the energies and eigenvectors associated with renormalized free problem, $\mathbf{M}_{\text{eff}}(\mathbf{k})$, not the original $\mathbf{M}(\mathbf{k})$. The renormalization, $\delta\mathbf{M}(\mathbf{k})$, is then chosen to cancel the static, Hartree-Fock-like contributions to the self-energy. This procedure does not strictly include only $O(1/S^2)$ contributions and is thus in some sense uncontrolled. However, using such an approach we can account for some of the change in the one-magnon energies due to interactions in the free problem, as well as access regions of the phase diagram outside the usual classical phase boundaries, without having to go to higher order in $1/S$.

Applied to the problem at hand, for the bulk case we assume the system is in the fully field polarized state with the magnetic moments aligned with the applied [111] field. Due to the anisotropic Kitaev exchange, even in this colinear state there are both three- and four-magnon interactions. The three-magnon interactions generically induce spontaneous decay of the one-magnon excitations when they overlap with the two-magnon continuum [13].

Our implementation considers a finite system of size $N = 2L^2$. We first solve for $\delta\mathbf{M}(\mathbf{k})$ for each wave-vector through self-consistent iteration (terminating when the maximum change in the correction is $\lesssim 10^{-8}$). In the classically allowed regions we can initialize the iteration trivially with $\delta\mathbf{M}(\mathbf{k}) = 0$. However, to access the critical field $h_c = 2$ for $K = +1$, we begin with small chemical potential $\delta\mathbf{M}(\mathbf{k}) = \mu\mathbf{1}$ where $\mu \sim 0.1$ to avoid the classical instability (the final result is independent of the choice of μ). Once $\mathbf{M}_{\text{eff}}(\mathbf{k})$ is determined for each wave-vector, we then compute $\boldsymbol{\Sigma}_{\mathbf{M}_{\text{eff}}}(\mathbf{k}, \omega)$ on a fine grid in frequency, including a small width $0^+ \rightarrow 10^{-3}$ to resolve any singularities. Performing the inversion in Eq. (44) numerically (including again a small width), we then obtain $\mathbf{G}(\mathbf{k}, \omega)$ which determines the dominant transverse-transverse part of the dynamical structure factor. The remaining free Green's functions and sums involved in the remaining parts [9] are evaluated similarly. The results in the main text show the full dynamical structure factor $S(\mathbf{k}, \omega)$ (as given in Eq. (3) of the main text) including the transverse-transverse, transverse-longitudinal and longitudinal-longitudinal contributions.

For the case with open boundaries we consider systems of $N = 2LW$ sites where $W = 5$, following the same strategy to evaluate the dynamical structure factor as in the bulk case. The main modification necessary arises at the classical level from the presence of open boundaries. Since the spins at the boundaries have fewer neighbors than those in the bulk, the classical ground state is no longer uniform, with the moment direction deviating from $[111]$ as one approaches the edges. Due to the lower symmetry, the static tadpole diagrams are non-zero and are included in the self-consistent iteration described above. The presence of these diagrams implies that the one-magnon expectation values do not vanish and thus there is finite $O(1/S^2)$ correction to the canting of the moments away from $[111]$. In addition, due to the imposition of open boundaries, the classical critical field is also lowered, with $h_c < 2$ for $K = +1$. As for the bulk case, the results in the main text show the layer-resolved dynamical structure factor, including the transverse-transverse, transverse-longitudinal and longitudinal contributions. To compare directly with the DMRG results, the definition of the layer-dependent structure factor only includes $S^{xx}(\mathbf{k}, \omega)$, as described in Fig. 3 of the main text.

IV. BULK DYNAMICAL STRUCTURE FACTORS

Fig. 4 shows the dynamical structure factors for $h = 2, 3, 4$ at the antiferromagnetic Kitaev point using linear spin wave theory, interacting spin wave theory to $1/S^2$ and time dependent DMRG along high symmetry lines. The results for $h = 3$ are shown in the main text. Linear spin wave theory disagrees significantly at all these fields - the bandwidth is overestimated - while interacting spin wave theory to $1/S^2$ agrees very well at $h = 3$ and $h = 4$ with the DMRG. At $h = 2$ the lowest magnon band is a flat band at zero energy (the calculation here is actually for $h = 2 + \epsilon$) while the fully polarized state is stable in the interacting spin wave calculation. However, at $h = 2$ the $1/S^2$ and DMRG calculations are mutually inconsistent in both the single magnons and the higher energy continuum scattering. Exact diagonalization results for the 24 site hexagonal cluster in the single magnon sector agree very well with the DMRG.

A similarly organized set of figures are shown for the ferromagnetic Kitaev point at $h = 1, 2$. While linear spin wave theory has the symmetry explained in Section II A, matching the spectra at the ferromagnetic and antiferromagnetic Kitaev points, this mapping breaks down in the presence of interactions and, indeed, the $\vartheta = \pi/2$ and $3\pi/2$ results are dramatically different. In particular, a multiparticle continuum visibly overlaps the upper single magnon bands in the DMRG causing considerable broadening. This is partially captured within interacting spin wave theory.

We draw the attention of the reader to the high intensity broad and nearly flat intensity visible at $h = 2$ in the DMRG around $\omega = 3$ (panel 4(c) in the top row). This feature of the multimagnon intensity persists to higher fields. The precise nature of this object is a question that we leave for future work.

V. DYNAMICAL CORRELATIONS IN THE SLAB GEOMETRY

Here we report further slab geometry results for the dynamical correlations as computed using linear spin wave theory, interacting spin wave theory and time dependent DMRG. The slab is described in the main text and illustrated at the bottom of Fig. 3 there.

Fig. 6 shows results at the antiferromagnetic Kitaev point at $h = 2$ (top) and $h = 4$ (bottom). The case of $h = 3$ is given in the main text. At $h = 4$ the finite size progenitor of the chiral mode on the semi-infinite slab is clearly visible in panel (a)(left) running between the bulk bands with highest intensity to the left of that panel. The principal result of including interactions is a narrowing of the bandwidth: the same mode being visible in (b) and (c). The middle of the slab has visible but lower intensity between those bands that persist into the bulk geometry. The lower set of panels again show the chiral mode - this time on the right of each panel. At $h = 2$, interactions play a much larger role because the lower threshold to two magnon states begins within the upper single magnon bands. The result is that there is considerable broadening of the upper single magnon modes. Nevertheless, the edge state appears to survive the presence of interactions.

The symmetry between noninteracting magnon spectra in the bulk under $\vartheta \rightarrow \vartheta + \pi$ ceases to hold on the slab geometry because the presence of an edge causes the ground states to be affected by the change in the coupling. We find that the chiral edge mode on the open geometry is not as clearly visible in the ferromagnetic Kitaev model as it is in the antiferromagnetic case. In Fig. 7 the chiral mode appears as inter-bulk band intensity in panel (a) with the same sign of the velocity as in (a) of Fig. 6. At $h = 2$, interactions bring about a fairly mild renormalization of the bands while, at $h = 1$, the multimagnon continua are clearly visible. The upper bulk single magnon modes are destroyed through coupling to these additional states while the whole block of single magnon states is pushed to lower energies. Despite this dramatic effect of interactions, once again, the edge mode appears to survive.

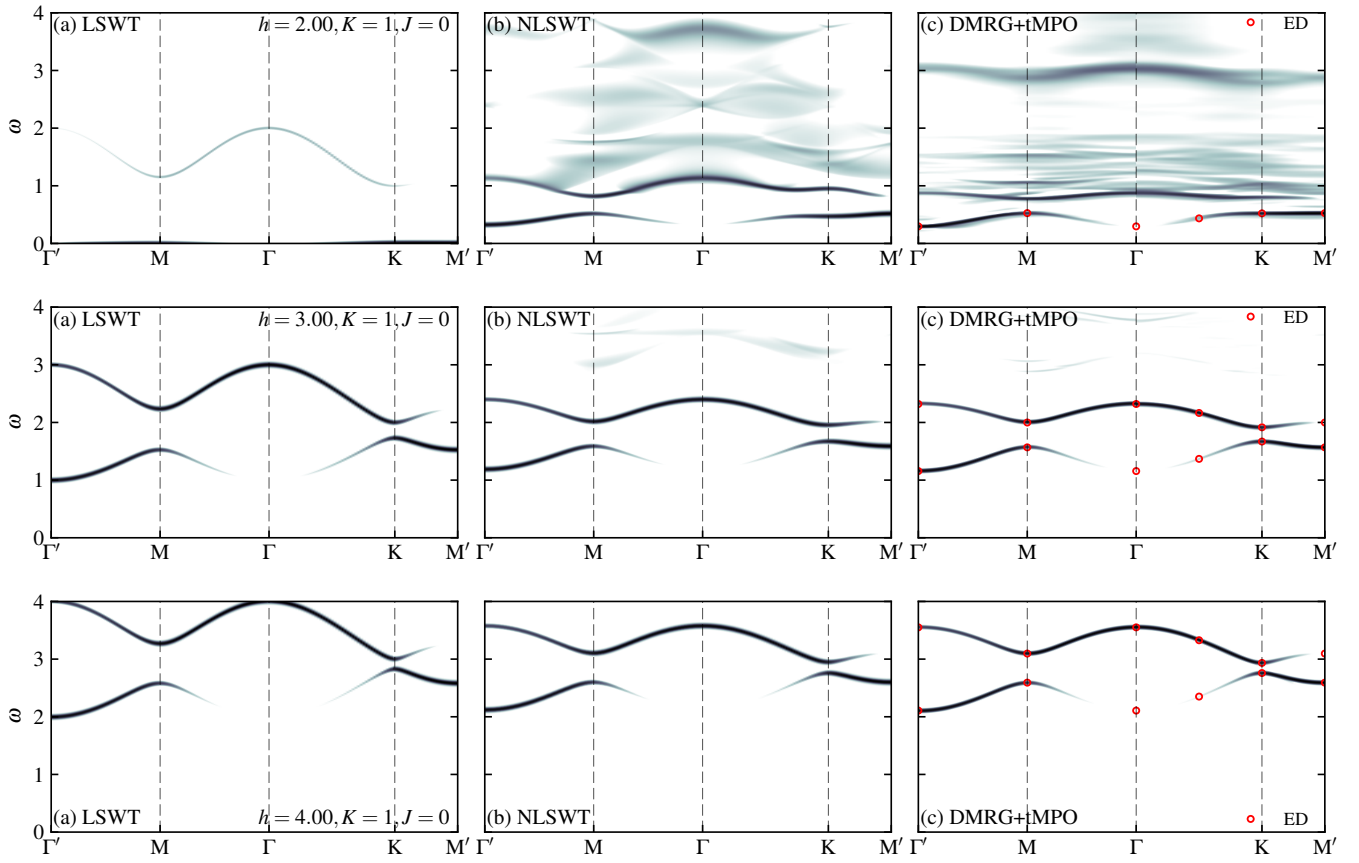


FIG. 4. Dynamical structure factor at the antiferromagnetic Kitaev point $\vartheta = \pi/2$ at fields $h = 2, 3, 4$ from top to bottom. The $h = 3$ figure appears also in the main text. The intensity scale is logarithmic from 5×10^{-3} to 1. At each field, results are shown for linear spin wave theory (left), nonlinear spin wave theory (middle) and time dependent DMRG (right). The red points in the right-hand plots are exact diagonalization results for the symmetric 24 site cluster. Most of the spectral weight for the LSWT calculation at $h = 2$ lies in the zero mode.

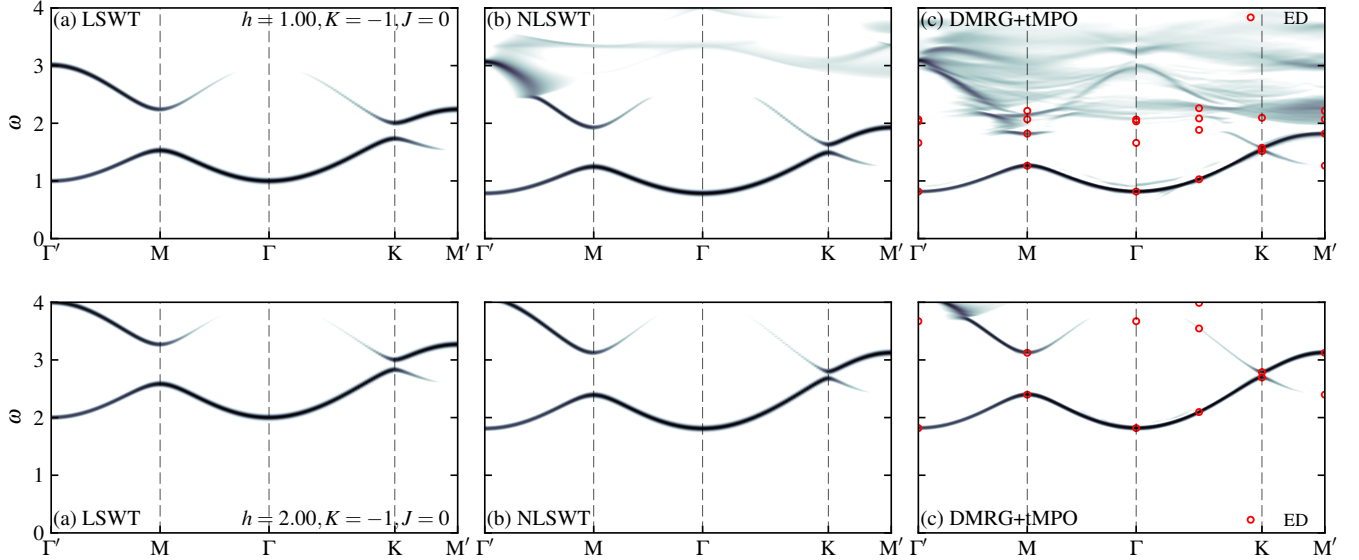


FIG. 5. Dynamical structure factor at the ferromagnetic Kitaev point $\vartheta = 3\pi/2$ at fields $h = 1, 2$ from top to bottom. The intensity scale is logarithmic from 5×10^{-3} to 1. At each field, results are shown for linear spin wave theory (left), nonlinear spin wave theory (middle) and time dependent DMRG (right).

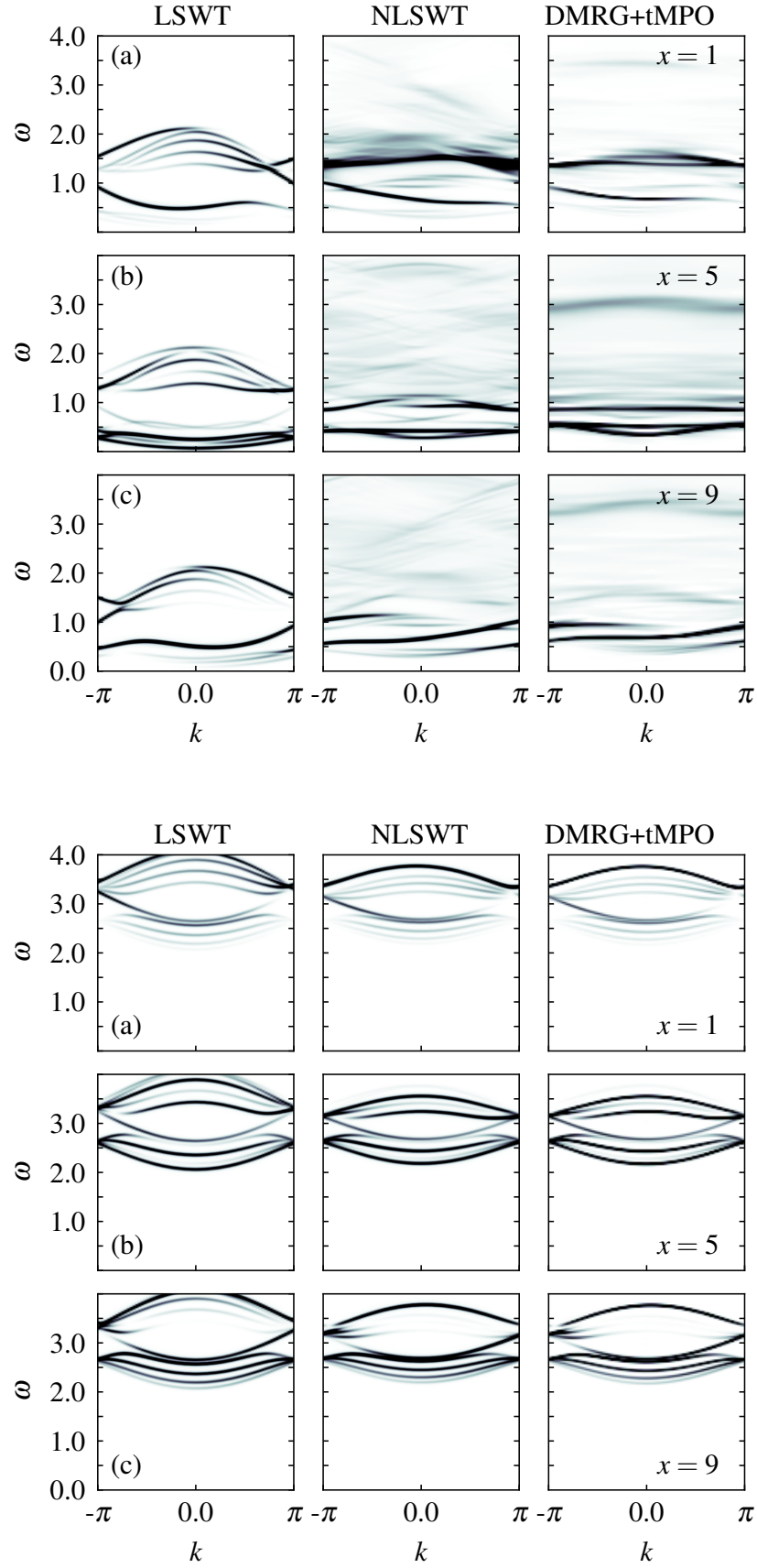


FIG. 6. Dynamical correlations on a slab geometry at the antiferromagnetic Kitaev point $\vartheta = \pi/2$ at fields $h = 2, 4$ from top to bottom. At each field, results are shown for linear spin wave theory (left), nonlinear spin wave theory (middle) and time dependent DMRG (right).

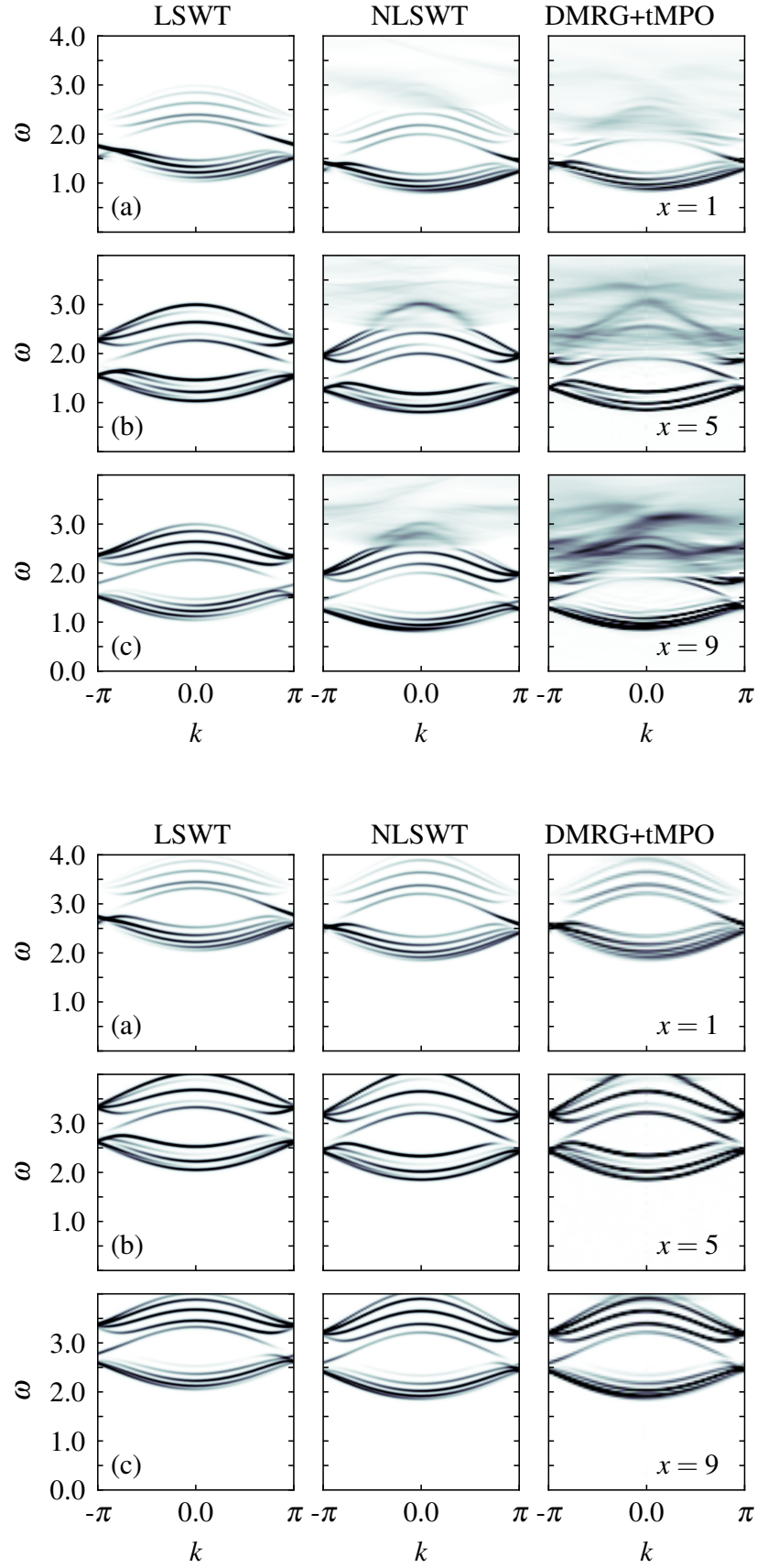


FIG. 7. Dynamical correlations on a slab geometry at the ferromagnetic Kitaev point $\vartheta = \pi/2$ at fields $h = 2, 4$ from top to bottom. At each field, results are shown for linear spin wave theory (left), nonlinear spin wave theory (middle) and time dependent DMRG (right).

-
- [1] V. M. Katukuri, S. Nishimoto, V. Yushankhai, A. Stoyanova, H. Kandpal, S. Choi, R. Coldea, I. Rousochatzakis, L. Hozoi, and J. Van Den Brink, *New Journal of Physics* **16**, 013056 (2014).
 - [2] J. G. Rau, E. K.-H. Lee, and H.-Y. Kee, *Phys. Rev. Lett.* **112**, 077204 (2014).
 - [3] G. Jackeli and G. Khaliullin, *Phys. Rev. Lett.* **102**, 017205 (2009).
 - [4] J. Chaloupka, G. Jackeli, and G. Khaliullin, *Phys. Rev. Lett.* **105**, 027204 (2010).
 - [5] L. Janssen, E. C. Andrade, and M. Vojta, *Phys. Rev. B* **96**, 064430 (2017).
 - [6] L. Janssen, E. C. Andrade, and M. Vojta, *Physical review letters* **117**, 277202 (2016).
 - [7] R. Matsumoto and S. Murakami, *Physical Review B* **84**, 184406 (2011).
 - [8] T. Holstein and H. Primakoff, *Phys. Rev.* **58**, 1098 (1940).
 - [9] M. Mourigal, W. T. Fuhrman, A. L. Chernyshev, and M. E. Zhitomirsky, *Phys. Rev. B* **88**, 094407 (2013).
 - [10] J.-P. Blaizot and G. Ripka, *Quantum theory of finite systems*, Vol. 3 (MIT press Cambridge, 1986).
 - [11] A. Chubukov, S. Sachdev, and T. Senthil, *Journal of Physics: Condensed Matter* **6**, 8891 (1994).
 - [12] A. L. Chernyshev and M. E. Zhitomirsky, *Phys. Rev. B* **79**, 144416 (2009).
 - [13] M. E. Zhitomirsky and A. L. Chernyshev, *Rev. Mod. Phys.* **85**, 219 (2013).